ISG15 induces IL-10 production in human monocytes and is a biomarker of disease severity during active tuberculosis

Paula Fernandes dos Santos[*], Johan Van Weyenbergh[¶], Murilo Delgobo[*], Daniel de Oliveira Patricio[*], Brian J. Ferguson[§], Rodrigo Guabiraba[#], Tim Dierckx[¶], Soraya Maria Menezes[¶], André Báfica[*★] and Daniel Santos Mansur[*★1]

*Laboratory of Immunobiology, Department of Microbiology, Immunology and Parasitology, Universidade Federal de Santa Catarina, Campus Trindade, Centro de Ciências Biológicas, Bloco A, sala 213, Santa Catarina, Brasil. CEP 88040-900

[§]Department of Pathology, University of Cambridge

[#]ISP, INRA, Université François Rabelais de Tours, 37380 Nouzilly, France

[¶]Department of Microbiology and Immunology, Rega Institute for Medical Research, Laboratory for Clinical and Epidemiological Virology, KU Leuven - University of Leuven, Leuven, Belgium

[1] Lead Contact

★Correspondence:

daniel.mansur@ufsc.br (D.S.M)

andre.bafica@ufsc.br (A.B.)

Running title

Human ISG15 drives a monocyte/IL-10 axis that is disrupted in active tuberculosis

Abstract (150 words)

Interferon stimulated gene 15 (ISG15) deficiency in humans leads to severe interferonopathies and mycobacterial disease, the latter being previously associated to its extracellular cytokine-like activity. Here, we demonstrate a novel role for secreted ISG15 as an IL-10 inducer, unique to human primary monocytes. Employing *ex vivo* systems analysis of human transcriptome datasets, we observed a significant correlation of ISG15-induced monocyte IL-10 and lymphocyte IFNγ balanced expression. This effect was associated with p38 MAPK and PI3K signalling in healthy volunteers. The specificity and MAPK/PI3K-dependence of ISG15-induced monocyte IL-10 production was confirmed *in vitro* using CRISPR/Cas9 knockout and pharmacological inhibitors. Moreover, this *ISG15*/*IL10* axis was amplified in leprosy but disrupted in human active tuberculosis (TB) patients. Importantly, ISG15 strongly correlated with inflammation and disease severity during active TB. In conclusion, this study identifies a novel anti-inflammatory ISG15/IL-10 myeloid axis that is disrupted in active TB, revealing a potential biomarker for disease severity in this major human disease.

Introduction

Type one interferons (IFN-I) exert most of their functions by inducing the expression of interferon-stimulated genes (ISGs). To date, over 300 ISGs have been described (de Veer et al., 2001; Der et al., 1998) and interferon stimulated gene of 15 KDa (ISG15) is prominently expressed in response to infection, in autoimmune diseases, cancer and physiological processes such as pregnancy (Dos Santos and Mansur, 2017; Hansen and Pru, 2014; Henkes et al., 2015; Hermann and Bogunovic, 2017; Tecalco Cruz and Mejia-Barreto, 2017; Wang et al., 2017a). ISG15 is synthesized as a 17 KDa precursor that is cleaved in the C-terminal region producing a mature form of 15 KDa. Also called ubiquitin cross-reactive protein (UCRP), ISG15 was the first ubiquitin-like protein to be described and it can be covalently linked to other proteins in a process called ISGylation (Dos Santos and Mansur, 2017; Haas et al., 1987; Loeb and Haas, 1992; Skaug and Chen, 2010). ISGylation is important for host defence against several viruses such as Influenza A, Vaccinia, Ebola, HIV and Hepatitis C virus in both human and mouse models (Morales and Lenschow, 2013; Schoggins and Rice, 2011; Skaug and Chen, 2010).

In addition to its intracellular ISGylation-mediated processes, the mature form of ISG15 can be secreted and possesses cytokine-like activities modulating leukocyte functions (Bogunovic et al., 2013; Dos Santos and Mansur, 2017). For instance, soluble ISG15 was found to enhance production of IFNγ by lymphocytes and NK cells (Bogunovic et al., 2012; D'Cunha et al., 1996) and to stimulate NK cell proliferation (D'Cunha et al., 1996) as well as neutrophil migration (Owhashi et al., 2003). Importantly, ISG15 deficiency in humans is associated with a severe Mendelian susceptibility to mycobacterial disease (Bogunovic et al., 2012) and cells from patients with a nonsense mutation or a frame-shift in *isg15* are deficient in IFNγ-

66 mediated immunity. This activity is attributed to the effects of extracellular ISG15 in
67 NK cells and possibly occurs through an unknown receptor (Bogunovic et al., 2012).
68 Furthermore, humans lacking ISG15 also develop exacerbated IFN-I-induced
69 immunopathology (Zhang et al., 2015). This evidence suggests that extracellular or
70 free ISG15 may regulate multiple aspects of the host immune response to pathogens
71 and implicate this protein as an important component induced during infection and/or
72 inflammatory processes involving IFN-I signalling. However, despite its ability to
73 induce pro-inflammatory mediators, IFN-I may also display opposing anti-
74 inflammatory effects (Billiau, 2006; Borden et al., 2007; McNab et al., 2015).
75 Nevertheless, whether soluble extracellular ISG15 modulates anti-inflammatory
76 responses has not been reported.
77 The present study demonstrates that ISG15 induces IL-10 synthesis in human primary
78 monocytes through MAPK- and PI3K-dependent pathways. Additionally, analysis of
79 human transcriptome data sets identified a myeloid *ISG15*/*IL10* axis present in
80 homeostasis. In contrast, the *ISG15*/*IL10* axis is disrupted during active TB and
81 *ISG15* mRNA levels strongly correlate with inflammatory and disease severity
82 markers. These data suggest ISG15 may play a role in the crosstalk between Type
83 I/Type II IFNs and IL-10 and reveal *ISG15* mRNA levels as potentially useful
84 biomarker in human active TB.
85

86 **Results and Discussion**

87 *ISG15 induces IL-10 production in human PBMC*

88 Extracellular ISG15 stimulates IFNγ production by human NK cells (Bogunovic et
89 al., 2012), so to investigate whether ISG15 regulates synthesis of other inflammatory
90 cytokines, PBMCs were exposed to soluble ISG15 and 24h cell culture supernatants
91 assayed for several cytokines by cytometric bead array (CBA). Out of this panel, only
92 IL-10 and IL-6 were induced by ISG15 (Supplementary figure 1A). IL-10 is a key
93 immune-regulatory cytokine that exerts opposing effects to IFNγ, hence this result
94 was further assessed by treating PBMCs with different concentrations of pro- or
95 mature ISG15 indicating a concentration-dependent response (Figure 1A). Following
96 intracellular processing of pro-ISG15, its C-terminal LRLRGG domain is exposed
97 and the protein becomes mature, a necessary requirement for ISGylation (Knight et
98 al., 1988; Loeb and Haas, 1992; Narasimhan et al., 1996; Potter et al., 1999). Both
99 pro- and mature ISG15 induced IL-10 secretion in human PBMCs in a similar manner
100 (Figure 1A), indicating that LRLRGG sequence does not need to be exposed for
101 ISG15-mediated IL-10 production. Exogenous ISG15 stimulated IL-10 synthesis by
102 PBMCs from most of the healthy donors tested (Figure 1B). Control experiments
103 showed that heat denatured ISG15 did not promote IL-10 synthesis demonstrating this
104 protein requires its folded structure to induce cell signalling (Figure 1B). Kinetic
105 analysis of ISG15-stimulation in human PBMCs showed a peak of IL-10 mRNA and
106 protein synthesis after 6 and 12 hours respectively (Figure 1C and D). Interestingly,
107 this response was found to be specific for primary cells as a library of human cell
108 lines (NKL, NK92, THP-1, Karpas, U937 and Jurkat) treated with ISG15 did not
109 produce IL-10 (data not shown). Additionally, ISG15 treatment did not induce cell
110 death by means of annexin V expression and propidium iodide (PI) incorporation

111 (Figure 1E-G) suggesting IL-10 was actively secreted, not released from nor induced
112 by apoptotic or necrotic cells. Together, these data show that ISG15 induces IL-10
113 synthesis and secretion by primary human PBMCs, independent of cell death.
114
115 *CD14$^+$ cells are the main producers of ISG15-induced IL-10*
116 ISG15 can act on different cell types (Bogunovic et al., 2012; D'Cunha et al., 1996;
117 Owhashi et al., 2003; Recht et al., 1991) hence intracellular cytokine staining was
118 used to identify the source of ISG15-induced IL-10 in PBMCs subpopulations. These
119 experiments indicated that a CD14$^+$ population is the main source of IL-10 (Figure
120 2A) with an average 2.5 fold-increase of CD14$^+$IL-10$^+$ cells as compared to
121 unstimulated cultures (Figure 2B). Next, PBMCs were separated into CD14$^+$ and
122 CD14$^-$ populations and both groups were exposed to soluble ISG15. Quantification of
123 IL-10 and IFNγ 24 hours post stimulation confirmed CD14$^+$ population to be the main
124 producers of IL-10 (Figure 2C) whilst we corroborated previous work showing the
125 CD14$^-$ population to be the source of ISG15-induced IFNγ (Figure 2D) (Bogunovic et
126 al., 2012; D'Cunha et al., 1996). Additionally, these data indicate that recombinant
127 ISG15-induced IL-10 synthesis by CD14$^+$ populations does not require the presence
128 of CD14$^-$ cells.
129 To test whether endogenously produced ISG15 stimulates IL-10 synthesis, a co-
130 culture experiment was set up using a lung epithelial cell line, A549, as a source of
131 ISG15 (Wang et al., 2017b). For these assays, an *ISG15*-knockout (KO) A549 cell
132 line was generated using CRISPR/Cas9 technology (Supplementary Figure 1B, clone
133 3). Wild type (WT) or *ISG15*-KO A549 cells were then co-cultured with purified
134 human primary CD14$^+$ cells or stimulated with LPS as a positive control. In this
135 setup, A549-monocyte co-cultures led to a consistent production of IL-10, an outcome

136 completely abrogated when *ISG15*-KO A549 cells were used. This effect could be
137 rescued by re-introduction of the *ISG15* gene into the knockout cells (Figure 2E) thus
138 demonstrating the specificity of epithelial cell-derived ISG15 for the induction IL-10.
139 To study co-regulation of *ISG15*/*IL10*/*IFNG* pathways in different cell types *ex vivo*,
140 we next examined transcriptome datasets of purified major human leukocyte subsets
141 (ImmuCo, ImmuSort) (Wang et al., 2015a; Wang et al., 2015b). Expression levels of
142 *ISG15* and *IL10* are positively correlated in total PBMCs, purified monocytes and
143 macrophages, but not neutrophils and T-cells (Figures 2F-J). Although neutrophils
144 display the highest *ISG15*/*IL10* expression ratio, monocytes are the main *ex vivo IL10*
145 expressing cell type (60.19% of cells with IL10 transcripts above detection limit, vs.
146 17.33% in PBMCs and 5.97% in neutrophils, Fig. 2K), thus corroborating with earlier
147 *in vitro* results (Fig. 2A-D). Consistent with a previous study (Tamassia et al., 2013),
148 low or undetectable *IL10* transcripts in human neutrophils (Fig. 2K) are explained by
149 the inactive chromatin configuration of the *IL10* locus in these cells. Together, this set
150 of results suggests a role for extracellular rather than intracellular ISG15 as inducer of
151 monocyte-derived IL-10 (this study) and NK-derived IFNγ (Bogunovic et al., 2012).
152 Since the unique susceptibility of ISG15-deficient children to low virulence
153 mycobacteria has underscored a role for extracellular ISG15 (Bogunovic et al., 2012),
154 we performed a systems analysis approach to gain insights on the possible influence
155 of ISG15/IL-10 axis during mycobacterial exposure in humans.
156
157

158 *IL-10 production in response to ISG15 requires MAPK-PI3K signalling pathways*

159 Mitogen-activated protein kinase (MAPK) and phosphatidylinositol-4,5-bisphosphate
160 3-kinase (PI3K) signalling pathways have been shown to participate in *IL10*
161 transcription in human monocytes and macrophages. For instance, p38, ERK1/2 and
162 PI3K are crucial for IL-10 synthesis during microbial stimuli such as LPS and
163 *Mycobacterium* (Ma et al., 2001; Nair et al., 2009). Thus, we analysed a published
164 transcriptome dataset of latent TB using WebGEstalt and Ingenuity Pathway Analysis
165 (IPA). As shown in Supplementary Table, MAPK and PI3K signalling pathways were
166 significantly enriched in latent TB transcriptomes, as compared to healthy, uninfected
167 controls. We next investigated whether members of MAPK and PI3K signalling
168 families displayed divergent expression patterns between latent and active TB. MAPK
169 family members were up-regulated in both latent and active TB (Figure 3A).
170 However, *PIK3CA* (PI3Kalpha) levels were up-regulated in active TB and down-
171 regulated in latent TB. In this scenario *MAPK14* (p38) expression levels were
172 significantly and positively correlated to *ISG15* levels *ex vivo* (Figure 3B).
173 Additionally, *MAPK3* (MAP3K/ERK1) levels were positively correlated to *IL10*
174 (Figure 3C) and negatively correlated to *IFNG* transcript levels (Figure 3D). Finally,
175 *PIK3CA* and *PIK3CB* (PI3Kbeta) transcripts were negatively correlated to *IL10*
176 expression levels (Figure 3E). These data suggested that ISG15/IL-10 as well as
177 MAPK/PI3K-associated transcripts are co-regulated during mycobacterial stimulation
178 *in vivo* and raised the possibility that MAPK/PI3K pathway is involved in ISG15-
179 induced IL-10 responses in monocytes. Indeed, following exposure of $CD14^+$ cells to
180 ISG15, increased phosphorylation of p38 MAPK was observed (Figure 3F). More
181 importantly, the use of two distinct inhibitors for p38 (Figures 3G-H) as well as
182 inhibitors for MEK1/2 (Figure 3I) and PI3K (Figure 3J) abrogated IL-10 production

183 in ISG15-stimulated monocytes. In contrast, chloroquine, an inhibitor targeting DNA-
184 PKCs/TLR9/endosome signalling pathways, did not affect IL-10 synthesis induced by
185 ISG15 (Figure 3J). These results suggest a central role for p38 activation and MAPK
186 as well as PI3K signalling in ISG15-induced IL-10 production by primary monocytes.
187
188 *An ISG15/IL10/IFNG cluster in healthy controls is disrupted during active TB*
189 Altogether, our data indicated that ISG15 is associated with immunoregulatory
190 responses and it could have an important role in mycobacterial-induced inflammation.
191 To test this concept, publicly available transcriptome data sets from established
192 cohorts of healthy controls and patients with leprosy as well as latent or active
193 tuberculosis were examined. Positive and negative correlations (Spearman Rho) were
194 calculated between normalized transcript levels of MAPK/PI3K/STAT signalling
195 family members, established myeloid lineage markers (*CD14*,
196 CD16=*FCGR3A/FCGR3B*, *ITGAM*, *ITGAX*) and lymphoid lineage markers (*CD4*,
197 *CD8*, CD56=*NCAM1*, *ITGAL*) plus *ISG15*, *IL10* and *IFNG* transcripts. Unsupervised
198 hierarchical clustering of these transcripts was then performed, based on the resulting
199 correlation matrices. In healthy controls (Figure 4A), *ISG15* mRNA strongly clusters
200 with *IL10*, and to a lesser extent with *IFNG*, indicating the existence of a regulatory
201 balance between pro-and anti-inflammatory effects under homeostatic conditions.
202 Leprosy lesions have been shown to express both type I IFN and IL-10, a scenario
203 that leads to suppression of IFNγ effector activities (Teles et al., 2013). An
204 unsupervised hierarchical cluster analysis of the cohort published by Teles and
205 colleagues shows the myeloid anti-inflammatory *ISG15*/*IL10* axis maintained in
206 leprosy lesions (Figure 4B), demonstrated by a single expression cluster comprised of,
207 *ISG15*, *IL10* and monocyte (*CD14*) and myeloid markers (CD64=*FCGR1*,

208 CD11c=*ITGAX*, PU.1=*SPI1*, CD16=*FCGR3*). Consistent with previous data (Teles et
209 al., 2013), this disease cluster was negatively correlated to a "protective"
210 *CD8*/*IFNG*/*STAT4* cluster, which is associated with milder (borderline
211 tuberculoid/paucibacillary) clinical form, whereas the *ISG15*/*IL10*/*CD14* cluster was
212 associated with the severe (lepromatous/multibacillary) disease form. Surprisingly,
213 the *ISG15*/*IL10* axis was disrupted in whole blood transcriptomes of active TB
214 (Figure 4C). However, ISG15 (but not *IL10* or *IFNG*) retained its association with
215 disease status and monocyte/myeloid markers (*CD14, FCGR1*). Since TB disease
216 signature in the whole blood is predominated by neutrophils (Berry et al., 2010) and
217 monocytes only make up a minor fraction in these samples, we next investigated
218 whether components of the *ISG15*/*IL10* signalling pathway might be overexpressed in
219 purified monocytes from TB patients, as compared to control monocytes. Indeed,
220 Ingenuity Pathway Analysis identified MAPK signalling as significantly enriched in
221 monocytes from TB patients (Supplementary Table), and p38 MAPK was
222 significantly interconnected with several TB signature genes (*FCGR1, IL27,*
223 *SIGLEC6*) in a disease network (Figure 4D). Together, these results show the
224 *ISG15/IL10* axis is disrupted during active TB.
225 To further investigate the possible connection between ISG15 and *M. tuberculosis*-
226 mediated immunopathology, we examined the expression of this gene in an
227 independent large cohort in which both detailed clinical parameters and
228 corresponding transcriptome data are available (Berry et al., 2010). Expression levels
229 of *ISG15* were significantly correlated with established inflammatory biomarkers such
230 as erythrocyte sedimentation rate (ESR), C-reactive protein (CRP), tissue damage
231 (Modal X-ray grade) as well as systemic clinical parameters (neutrophil count,

232 haemoglobin, and globulin serum concentration) (Figure 4 G-L). These results
233 suggest ISG15 is a sensitive biomarker of disease severity in active TB patients.
234 ISG15 is critical for the production of IFNγ in cells from vaccine strain *BCG*-infected
235 patients (Bogunovic et al., 2012). Moreover, ISG15 has a synergistic effect when
236 combined with IL-12 (Bogunovic et al., 2012), an important inducer of IFNγ (Chan et
237 al., 1992; Chan et al., 1991). Furthermore, IL-10 inhibits production of IL-12 and,
238 consequently, of IFNγ by PBMCs (D'Andrea et al., 1993), pointing to a pleiotropic
239 effect for ISG15. Cell type and context dependent effects of ISG15 could explain
240 these diverse activities. This work and others (Bogunovic et al., 2012) suggest that
241 despite ubiquitous expression in different cell types, neutrophils are the major source
242 of secreted ISG15. Although we have not tested this directly, we speculate that
243 soluble neutrophil-derived ISG15 places neutrophils as pivotal to the orchestration of
244 immune responses *in vivo*, driving the production of at least two major cytokines, IL-
245 10 and IFNγ. Interestingly, the intra and extracellular location of ISG15 and its
246 ability to induce a plethora of effects in distinct cells, resembles the function of an
247 alarmin (Rider et al., 2017). As shown in figure 4, ISG15's function is context
248 dependent, varying from a driver of an anti-inflammatory monocytic/IL-10 axis in
249 homeostasis and the less severe *M. leprae* infection to a strong pro-inflammatory
250 IFNγ-biased scenario during active TB. Whether virulent *M. tuberculosis* hijacks the
251 ISG15/IL-10 axis contributing to induction of tissue pathology remains to be
252 determined.
253 In conclusion, these findings confirm and extend previous work characterizing soluble
254 extracellular ISG15 as a pleiotropic cytokine (or alarmin) that induces both pro- and
255 anti-inflammatory effects in a variety of cell types. Moreover, the combined *ex vivo*
256 and *in vitro* approach uncovers a novel myeloid *ISG15*/*IL10* p38-mediated anti-

257 inflammatory signalling cascade, which is preserved in human leprosy but disrupted
258 in active TB. Strikingly, our data indicate *ISG15* mRNA as a novel biomarker of
259 disease severity during acute TB that merits further investigation.
260

261 **Figure Legends**

262 **FIGURE 1** – ISG15 induces the production of IL-10 in human PBMCs. (**A**) Dose-
263 dependent IL-10 production as measured by ELISA 24 hours post stimulation of
264 PBMCs with both pro- and mature ISG15 ([ISG15]: 0.15; 0.45; 1.5, 4.5 and 15
265 μg/mL). (**B**) Induction of IL-10 by recombinant, but not heat-treated, ISG15 using
266 PBMCs from a total of 5 different donors in 8 independent experiments. (**C**) *IL10*
267 mRNA expression in PBMCs treated with ISG15 at 6, 12, 24 and 48 hours post
268 stimulation. (**D**) Quantification of IL-10 in the supernatant of human PBMCs at 6, 12,
269 24 and 48 hours after treatment with of ISG15 (**E**) Representative dot-plot evaluating
270 cell-death in human PBMCs by annexin V and PI staining after treatment with ISG15
271 (2.0 μg/m) or Staurosporine (1 μM). (**F, G**) Quantification of cell death from the
272 experiment described in (**E**). Unless stated otherwise, ISG15 concentration was 1.5
273 μg/mL. Error bars indicate SEM for biological replicates in each experiment. In each
274 experiment PBMCs from 3 or more different donors were used. * P-value<0.05, ** p-
275 value<0.01 and **** p-value<0.0001. ISG15HT, ISG15 heat-treated; STA,
276 Staurosporine; PI, Propidium Iodide; Uns, Unstimulated.

277

278 **FIGURE 2** – $CD14^+$ cells are the main source of IL-10 upon ISG15 stimulation. (**A**)
279 Representative dot plot of intracellular staining of IL-10 in $CD14^+$, $CD56^+$, $CD4^+$ and
280 $CD8^+$ in ISG15-treated PBMCs. (**B**) PBMCs from 6 different individuals showing
281 fold increase in IL-10 production from $CD14^+$, $CD56^+$, $CD4^+$ and $CD8^+$ populations
282 after ISG15 stimulation. (**C-D**) ELISA quantification of IL-10 and IFNγ in the
283 supernatants of $CD14^+$ and $CD14^-$ separated populations treated with ISG15 (**E**)
284 A549 WT or ISG15 KO cells were co-cultured with primary $CD14^+$ cells
285 magnetically separated from PBMCs and IL-10 production was measured by ELISA

286 24 hours later. *ISG15* KO cells were also transfected with a plasmid expressing *ISG15*
287 in order to rescue its function. LPS was used as a positive control for IL-10
288 stimulation. Error bars indicate SEM for biological replicates in each experiment. All
289 experiments were repeated at least two times. In every experiment PBMCs from 3 or
290 more donors were used. (**F-J**) Transcriptome datasets of healthy controls (ImmuCo,
291 ImmuSort) confirm *ISG15* and *IL10 ex vivo* expression levels are strongly and
292 positively correlated in total PBMCs (**F**), purified primary monocytes (G) and
293 macrophages (**H**), but not neutrophils (**I**) or T cells (**J**). Red lines indicate the
294 approximate threshold for *IL10* mRNA detection (determined for each individual
295 microarray). (**J**) Neutrophils display the largest *ISG15*/*IL10* ratio *ex vivo*, whereas
296 monocytes are the major *IL10* expressing leukocyte population
297 (>PBMCs>neutrophils) under homeostatic conditions. **** p-value<0.0001.
298
299 **FIGURE 3**: ISG15 induces monocyte derived IL-10 via p38, MEK1/2 and PI3K
300 signalling pathways, which are deregulated in human mycobacterial infections. (**A**)
301 MAPK family members expression in both latent and active TB. *Ex vivo* expression
302 levels correlation of *MAPK14* and *ISG15* (**B**), *MAPK3* and *IL-10* (**C**), *MAPK3* and
303 *IFNG* (**D**) and of *PIK3CA* or *PIK3CB* with *IL-10* (**E**) during latent TB infection (**F**)
304 Representative immunoblot showing the phosphorylation of p38 MAPK 15 min after
305 the stimulation of ISG15 in $CD14^+$ cells. (**G-J**) $CD14^+$ cells were treated for 1h with
306 p38 (10 µM), MEK1/2 (50 µM) and PI3K inhibitors (50 µM) (B-E respectively) prior
307 to addition of ISG15 (1µg/mL) or LPS (100 ng/mL). (**K**) Chloroquine (5µg/mL) was
308 used as an unrelated control drug. 24 hours after treatment, supernatant was harvested
309 and used for IL-10 quantification by ELISA. Error bars indicate SEM for biological

310 replicates in two independent experiments. * P-value<0.05, ** p-value<0.01 and ***
311 p-value<0.001. Uns, Unstimulated.
312
313 **FIGURE 4:** An anti-inflammatory *ISG15*/*IL10* myeloid axis is amplified in human
314 leprosy and disrupted in human tuberculosis, revealing a novel clinical biomarker. (**A-**
315 **C**) Heatmaps representing positive (red) and negative (blue) correlation matrix of
316 selected genes (see text) classified by unsupervised hierarchical clustering (Eucledian
317 distance). (**A**) Healthy controls (GSE80008) (**B**) Leprosy patients (GSE82160) (**C**)
318 TB cohort (GSE85487) (**D**) Significantly enriched network (Ingenuity Pathway
319 Analysis) showing p38 MAPK as highly interconnected in the monocyte
320 transcriptome of TB patients. (**E-F**) *ISG15* transcript correlates with (**G, H**)
321 established inflammatory metrics (erythrocyte sedimentation rate (ESR), C-reactive
322 protein (CRP), (**I**) tissue damage (Modal X-ray grade) as well as (**J-L**) systemic
323 clinical parameters (neutrophil count, haemoglobin, and globulin serum
324 concentration).
325
326 **Supplementary figure**
327 (**A**) ISG15 induces the production inflammatory cytokines. PBMCs from healthy
328 donors were treated with ISG15 (15 µg/mL) and supernatant was harvested 24 hours
329 for inflammatory cytokines quantification by cytometric Bead Array (CBA). ISG15
330 induced the production of IL-10, IL-6 and IL-1β. (**B**) Generation of ISG15 deficient
331 A549 cell line. ISG15 deficient A549 cell line was produced using CRISPR/Cas9.
332 After clone selection, cells were stimulated with IFNβ (1000 IU/mL), proteins
333 extracted after 24 hours and immunoblotted with anti-ISG15 and anti-tubulin
334 antibodies. Clone 3 (ISG15 KO) was used for further experiments.

335 **Supplementary Table**

336 Tab 1. PI3K gene expression enriched during latent tuberculosis.

337 Tab 2. MAPK gene expression enriched during latent tuberculosis.

338 Tab 3. Ingenuity Pathway Analysis for MAPK in monocytes during latent
339 tuberculosis.

340 Tab 4. p38 network in monocytes during active tuberculosis.

341

342 **Material and methods**

343 *Reagents*

344 ISG15 was purchased from Boston Biochem and tested for endotoxins by R&D
345 Systems (endotoxin value for lot #DBHF0614021 is <0.00394 EU/µg). LAL assay
346 (Lonza) was performed according to the manufacturer's instruction and the endotoxin
347 level of recombinant ISG15 was below the detection threshold. Pro-ISG15 (UL-615)
348 was also purchased from Boston Biochem. *E. coli* LPS (strain O111:B4) (Invivogen)
349 was used as a positive control for IL-10 production in human PBMCs and monocytes.
350 P38 kinase inhibitors SB203580 and SB220025 (Calbiochem) were used at 10 µM,
351 MEK1/2 inhibitor U0126 (Cell Signaling) at 50 µM and PI3K inhibitor Ly294002
352 (Cell Signaling) was at 50 µM. Solvent (DMSO, medium) was used as negative
353 control and chloroquine (Sigma, 5µg/mL), a DNA-PKC/TLR endosomal signalling
354 inhibitor, was used as an additional negative control.

355

356 *Primary human cells*

357 Human PBMCs were separated from healthy individuals using Ficoll-paque (GE)
358 according to manufacturer's instructions. Briefly, blood was collected in heparin-
359 containing tubes, and gently mixed 1:1 with saline solution and gently mixed before

360 being added over one volume of Ficoll-paque reagent. The gradient was centrifuged
361 for 35 minutes at 400 x g, 18˚C. PBMCs were harvested and washed once with 45 mL
362 of saline solution for 10 min at 400 x g, 18˚C. Subsequently, cell pellet was
363 suspended and washed twice with 5 mL of saline solution for 10 min at 200 x g, 18˚C
364 to remove platelets. The remaining cell pellet was suspended to the desired density in
365 RPMI 1640 (Gibco) supplemented with 5% foetal calf serum (Hyclone), 2mM L-
366 glutamine (Gibco), 1 mM sodium pyruvate (Gibco), 25 mM HEPES (Gibco), 100
367 U/mL penicillin and 100 µg/mL streptomycin (Gibco). Cells were plated as described
368 in each experiment. Human primary monocytes ($CD14^+$ cells) were separated from
369 PBMCs using CD14 microbeads (Miltenyi Biotec) according to manufacturer's
370 instructions with the exception of the MACS buffer, which was prepared using 3%
371 foetal calf serum. Monocyte enrichment varied between 73 to 92% between
372 experiments. The use of PBMCs from healthy donors was previously approved by
373 UFSC ethical committee (IRB#283/08).
374
375 *Generation of isg15 knockout cell lines*
376 A549 lung epithelial cells were co-transfected with three gRNA/Cas9/GFP plasmids
377 (provided by Horizon) targeting the *ISG15* locus using JetPEI (PolyPlus
378 Transfection). The guide RNAs used were 5' GGCTGTGGGCTGTGGGCTGT 3', 5'
379 GGTAAGGCAGATGTCACAGG 3' and 5' TGGAGCTGCTCAGGGACACC 3'.72
380 hours after transfection, cells sorted for GFP fluorescence and then separated by
381 limiting dilution. Single-cell derived clones were selected for ISG15 expression
382 (Supplementary Figure 1B).
383
384 *A549 – CD14+ co-culture*

385 A549 WT or ISG15 KO cells were seeded at 2 x 10^5 cells/ml in 24 well-plates. Cells
386 rested in the incubator for 6 hours before ISG15 KO cells were transfected with
387 ISG15-pCEP4 plasmid using FugeneHD reagent (Promega) according to
388 manufacturer's instructions. Cells were then washed and LPS was added 18 hours
389 after transfection and immediately prior to the addition of a 2 x 10^5 $CD14^+$ cells
390 overlay. Following 24 hours of co-culture, supernatants were harvested for IL-10
391 quantification.
392
393 *Immunoblotting*
394 1 x 10^5 $CD14^+$ cells were added to a 96-well plate and left to rest overnight. Cells
395 were stimulated with ISG15 (1μg/ml) and after 15 minutes cells were spun at 4˚C,
396 supernatant was removed and M-PER lysis buffer (Thermo Scientific) containing
397 protease inhibitors (Complete, Mini Protease Inhibitor Tablets, Roche) and
398 phosphatase inhibitors (#524625, Calbiochem) was added to the cells. Protein
399 separation was performed according to M-PER manufacturer's instructions.
400 Antibodies concentrations for detection of p38 (Cell Signaling #9212) and p-p38 (Cell
401 Signaling #9211), ISG15 (Cat: A600, R&D Systems) and anti-α-Tubulin (clone
402 DM1A, Millipore) were those suggested by the manufacturers. For Western blots, at
403 least 20 μg of total protein were separated and transferred to a PVDF 0.22 μm
404 blotting membrane. Membrane was blocked for at least 1 hour with 1X Tris Buffered
405 Saline-0.1% Tween20 (TBST) with 5% w/v non-fat dry milk and subsequently
406 washed 3 times with TBST for 5 minutes each wash. Membrane was incubated with
407 primary antibodies diluted in 5% w/v BSA, 1X TBS, 0.1% Tween20 at 4˚C with
408 gentle shaking overnight. Membrane was washed 3 times for 5 min each with TBST
409 and then incubated with the appropriate secondary HRP-linked antibody for 1 hour at

410 room temperature. Membrane was washed 3 times of 5 min each with TBST before
411 detection with ECL chemiluminescent substrate (Pierce).
412
413 *p38 MAPK and PI3K signalling pathway inhibition*
414 1 x 10^5 $CD14^+$ cells were added to a 96-well plate and left to rest overnight. Inhibitors
415 were added to cells for 1 hour prior to ISG15 treatment. 24 hours after treatment, cells
416 were spun at 4˚C; supernatant was harvested and IL-10 was quantified by ELISA.
417
418 *Cytokine quantification*
419 For exploratory experiments, IL-1β, IL-6, IL-10, IL-12p70 and TNF were quantified
420 in supernatants by human inflammatory cytokine cytometric beads array kit (CBA,
421 BD Biosciences). IL-10 and IFNγ were quantified using Human IL-10 DuoSet ELISA
422 kit (R&D Systems) or Human IFNγ mini kit (Thermo Scientific) according to
423 manufacturer's instructions.
424
425 *Flow Cytometry Assays*
426 PBMCs were seeded at a density of 5 x 10^5 cells per well in 150 µL of medium. After
427 8 hours of resting at 37°C with 5% CO_2, cells were treated with ISG15 (2 µg/mL) or
428 LPS (1 µg/mL), unless indicated otherwise. Golgi Plug protein transport inhibitor
429 (BD Biosciences) was added 1-hour post treatment, according to manufacturer's
430 instructions. Then, 12 hours post treatment; growth medium was removed and cold
431 1X HBSS (Gibco) with 2.5 mM EDTA was added to each well. The tissue culture
432 dish was kept at 4˚C for 30 minutes and cells were suspended and transferred to 1.5
433 mL tubes. Cells were washed in a final volume of 1mL cold 1X HBSS (Gibco) with
434 2.5 mM EDTA at 300 x g and 4˚C for 5 minutes. Supernatant was removed and cells

435 were suspended in FACS buffer (1% BSA, 1% sodium azide in 1X PBS). Anti-human
436 antibody mix containing anti-CD4 APC-Cy7 (clone OKT1) (BioLegend), anti-CD8
437 PE-Cy7 (clone SK1) (BioLegend), anti-CD14 PerCP-Cy5.5 (clone M5E2)
438 (BioLegend), anti-CD56 FITC (clone NCAM 16.2) (BD Biosciences) was added to
439 the cell suspension for 40 min at 4ºC in the presence of 10% AB blood-type human
440 serum to block Fc receptors. Afterwards, cells were washed once with 1 mL of 1X
441 PBS at 300 x g, 4˚C, for 5 minutes and 1 mL of fixation buffer (1% paraformaldehyde
442 in 1X PBS) was added to the cells. Tubes were kept in the dark at room temperature
443 for 15 min and then centrifuged at 300 x g, 4˚C, for 10 min to remove supernatant. 1
444 mL of permeabilization buffer (0.5% saponin in FACS buffer) was added to the cells
445 and tubes were centrifuged at 300 x g, 4 C for 10 min. Intracellular stain with anti-IL-
446 10-PE (clone JES3-9D7) (BioLegend) was carried out for 30 min in the dark at room
447 temperature. Cells were washed with permeabilization buffer at 300 x g, 4˚C, 5 min,
448 supernatant was removed and cells were suspended in FACS buffer prior to
449 acquisition of 1 x 10^5 events or more. For analysis, all acquired events displayed as
450 forward scatter (FSC) and side scatter (SSC) parameters were selected. After that,
451 single cells events were selected using FSC area and height parameters (FSC-A x
452 FCS-H) and auto-fluorescence was excluded using APC as an open channel.
453 Intracellular IL-10 was then quantified in monocytes ($CD14^+IL\text{-}10^+$), NK cells
454 ($CD56^+IL\text{-}10^+$), CD4 ($CD4^{high}IL\text{-}10^+$) and CD8 T cells ($CD8^{high}IL\text{-}10^+$). Gates were
455 set according to unstained PBMC sample and controls. All samples were acquired on
456 a Becton-Dickinson Verse flow cytometer using BD FACSuite™ software. In order
457 to analyse cell death, 5x10^5 PBMC/well were treated with ISG15 2 µg/mL or
458 Staurosporine (Sigma) 1 µM for 24 hours. Cells were then harvest, washed with 1 mL
459 of PBS at 300 x g, room temperature, 5 min, supernatant was removed and cells were

460 washed once in 1 mL of 1x Annexin biding buffer (eBioscience). Cell were
461 resuspended at 10^6 cells/mL in 1x Annexin biding buffer and FITC conjugated
462 Annexin V (eBioscience) was added to the cell suspension for 15 min, room
463 temperature, according to manufacture's instruction. Following incubation period,
464 cells were washed with 1 mL of 1x Annexin biding buffer, 300 x g, room
465 temperature, 5 min and resuspended in 200 uL of 1x annexin biding buffer. Propidium
466 iodide (BD Pharmingen) was added at 0.25 µg/mL to the cell suspension prior to
467 sample acquisition. Samples were acquired on a Becton-Dickinson Canto II flow
468 cytometer using BD FACSDiva™ software.
469
470 *Real time quantitative PCR (qPCR)*
471 For relative quantification of *IL10* gene expression, total RNA was extracted from
472 PBMCs treated or not with ISG15. RNA was extracted after 6, 12, 24 or 48 hours of
473 treatment using RNeasy RNA extraction kit (Qiagen). Using 400 ng of RNA, cDNA
474 was produced with High-Capacity cDNA Reverse Transcription Kit (Applied
475 Biosystems) and 2µL of the product was used for the qPCR reaction in a final volume
476 of 10 µL. qPCR reactions were performed using the primers forward 5'GAG ATC
477 TCC GAG ATG CCT TCA G 3'and reverse 5'CAA GGA CTC CTT TAA CAA
478 CAA GTT GT 3' (Skrzeczynska-Moncznik et al., 2008). Fold-increase in *IL10* gene
479 expression was determined by relative quantification using hypoxanthine
480 phosphoribosyltransferase (*HPRT*) as endogenous control. Primers forward and
481 reverse for *HPRT* were 5' CCTGCTGGATTACATCAAAGCACTG 3' and 5'
482 TCCAACACTTCGTGGGGTCCT 3', respectively, and were used at 250 nM each.
483
484 *Microarray analysis*

485 Curated and annotated publicly available data-sets (Berry et al., 2010; Novais et al.,
486 2015; Speake et al., 2015; Teles et al., 2013; Wang et al., 2015a; Wang et al.,
487 2015b)(GXB, ImmuCo, ImmuSort, BioGPS, GEO) were obtained from large,
488 established cohorts of healthy controls, latent and active tuberculosis patients,
489 comprising *ex vivo* and *in vitro* whole blood, total PBMCs, purified leukocyte subsets,
490 non-leukocyte human primary cells and skin biopsies (leprosy patients, healthy
491 controls and cutaneous leishmaniasis as non-mycobacterial infectious control). Novel
492 datasets were generated for both whole blood and PBMCs from healthy controls and
493 individuals infected with other non-mycobacterial intracellular pathogens
494 (*Leishmania*, HIV-1, HTLV-1). PBMCs were isolated as above and immediately
495 frozen in Trizol to preserve RNA integrity. Following Trizol extraction, total RNA
496 was further purified using an RNeasy kit according to the manufacturer's protocol
497 (QIAGEN, Venlo, Netherlands). Affymetrix Whole Genome microarray analysis was
498 performed by the VIB Nucleomics Facility (Leuven, Belgium) using a GeneChip®
499 Human Gene 1.0 ST Array with the WT PLUS reagent kit (Affymetrix, Santa Clara,
500 CA, USA) according to the manufacturer's specifications. Data preprocessing (RMA)
501 was performed using the Bioconductor xps package. All microarray raw data are
502 available at Gene Expression Omnibus database (GEO,
503 http://www.ncbi.nlm.nih.gov/geo/) under series accession numbers GSE80008,
504 GSE82160, GSE85487.
505
506 *Enrichment analysis*
507 The Ingenuity Pathway Analysis (IPA) program was used to perform the initial
508 pathway/function level analysis on genes determined to be differentially expressed in
509 the microarray analysis (Ingenuity Systems, Red Wood City, CA). Uncorrected p-

510 values and absolute fold-changes were used with cut-offs of $p<0.05$. Based on a
511 scientific literature database, the genes were sorted into gene networks and canonical
512 pathways, and significantly overrepresented pathways were identified. Further
513 enrichment analysis was performed, including Gene Ontology (GO) term enrichment
514 using the WEB-based GEne SeT AnaLysis Toolkit (WebGestalt), KEGG pathway
515 enrichment using the pathway database from the Kyoto Encyclopedia of Genes and
516 Genomes and transcription factor target enrichment using data from the Broad
517 Institute Molecular Signatures Database (MSigDB). Genesets from the GO, KEGG
518 pathways, WikiPathways and Pathway Commons databases, as well as transcription
519 factors, were considered overrepresented if their corrected p-value was smaller than
520 0.05. Principal component analysis, correlation matrices (Spearman), unsupervised
521 hierarchical (Eucledian distance) clustering were performed using XLSTAT and
522 visualized using MORPHEUS (https://software.broadinstitute.org/morpheus/).
523
524 *Data processing and statistical analyses*
525 Data derived from *in vitro* experiments was processed using Graphpad Prism 6 and
526 analysed using unpaired Student's T test unless stated otherwise. Statistical
527 significance is expressed as follows: * P-value<0.05, ** p-value<0.01, *** p-
528 value<0.001 and **** p-value<0.0001. In all cases, data shown are representative
529 from at least two independent experiments. Data from experiments performed in
530 triplicate are expressed as mean ± SEM.
531
532 **Acknowledgements**
533 DSM received support from CAPES Computational Biology (23038.010048/2013-
534 27), CNPq Universal (473897/2013-0) and the Academy of Medical Sciences/UK

(NAF004/1005). PFS and MD received CAPES and CNPq student fellowships respectively. AB received financial support from NIH-GRIP (TW008276), HHMI-ECS (55007412). AB is CNPq-PQ scholar and CAPES/ESE. BJF received support from an Isaac Newton Trust/Wellcome Trust ISSF/University of Cambridge research grant and a Wellcome Trust Seed Award (201946/Z/16/Z). TD received grant support from VLAIO (IWT141614). JVW received grant support from CAPES (PVE) and FWO (G0D6817N).

We would like to thank Prof. Aristobolo Mendes Silva from UFMG for providing reagents, suggestions and critical evaluation of these results.

The authors declare no conflict of interest.

Author contributions

PFS, JVW and RG designed, performed experiments, analysed the data and wrote the manuscript; MD, DOP, TD and SMM performed experiments and analysed the data, BF, AB and DSM designed experiments analysed the data and wrote the manuscript.

References

Berry, M.P., C.M. Graham, F.W. McNab, Z. Xu, S.A. Bloch, T. Oni, K.A. Wilkinson, R. Banchereau, J. Skinner, R.J. Wilkinson, C. Quinn, D. Blankenship, R. Dhawan, J.J. Cush, A. Mejias, O. Ramilo, O.M. Kon, V. Pascual, J. Banchereau, D. Chaussabel, and A. O'Garra. 2010. An interferon-inducible neutrophil-driven blood transcriptional signature in human tuberculosis. *Nature* 466:973-977.

Billiau, A. 2006. Anti-inflammatory properties of Type I interferons. *Antiviral research* 71:108-116.

Bogunovic, D., S. Boisson-Dupuis, and J.L. Casanova. 2013. ISG15: leading a double life as a secreted molecule. *Exp Mol Med* 45:e18.

Bogunovic, D., M. Byun, L.A. Durfee, A. Abhyankar, O. Sanal, D. Mansouri, S. Salem, I. Radovanovic, A.V. Grant, P. Adimi, N. Mansouri, S. Okada, V.L. Bryant, X.F. Kong, A. Kreins, M.M. Velez, B. Boisson, S. Khalilzadeh, U. Ozcelik, I.A. Darazam, J.W. Schoggins, C.M. Rice, S. Al-Muhsen, M. Behr, G. Vogt, A. Puel, J. Bustamante, P. Gros, J.M. Huibregtse, L. Abel, S. Boisson-Dupuis, and J.L. Casanova. 2012. Mycobacterial disease and impaired IFN-gamma

568 immunity in humans with inherited ISG15 deficiency. *Science* 337:1684-
569 1688.
570 Borden, E.C., G.C. Sen, G. Uze, R.H. Silverman, R.M. Ransohoff, G.R. Foster, and G.R.
571 Stark. 2007. Interferons at age 50: past, current and future impact on
572 biomedicine. *Nat Rev Drug Discov* 6:975-990.
573 Chan, S.H., M. Kobayashi, D. Santoli, B. Perussia, and G. Trinchieri. 1992.
574 Mechanisms of IFN-gamma induction by natural killer cell stimulatory
575 factor (NKSF/IL-12). Role of transcription and mRNA stability in the
576 synergistic interaction between NKSF and IL-2. *Journal of immunology*
577 148:92-98.
578 Chan, S.H., B. Perussia, J.W. Gupta, M. Kobayashi, M. Pospisil, H.A. Young, S.F.
579 Wolf, D. Young, S.C. Clark, and G. Trinchieri. 1991. Induction of interferon
580 gamma production by natural killer cell stimulatory factor:
581 characterization of the responder cells and synergy with other inducers.
582 *The Journal of experimental medicine* 173:869-879.
583 D'Cunha, J., E. Knight, Jr., A.L. Haas, R.L. Truitt, and E.C. Borden. 1996.
584 Immunoregulatory properties of ISG15, an interferon-induced cytokine.
585 *Proceedings of the National Academy of Sciences of the United States of*
586 *America* 93:211-215.
587 de Veer, M.J., M. Holko, M. Frevel, E. Walker, S. Der, J.M. Paranjape, R.H.
588 Silverman, and B.R. Williams. 2001. Functional classification of interferon-
589 stimulated genes identified using microarrays. *Journal of leukocyte biology*
590 69:912-920.
591 Der, S.D., A. Zhou, B.R. Williams, and R.H. Silverman. 1998. Identification of genes
592 differentially regulated by interferon alpha, beta, or gamma using
593 oligonucleotide arrays. *Proceedings of the National Academy of Sciences of*
594 *the United States of America* 95:15623-15628.
595 Dos Santos, P.F., and D.S. Mansur. 2017. Beyond ISGlylation: Functions of Free
596 Intracellular and Extracellular ISG15. *Journal of interferon & cytokine*
597 *research : the official journal of the International Society for Interferon and*
598 *Cytokine Research*
599 Haas, A.L., P. Ahrens, P.M. Bright, and H. Ankel. 1987. Interferon induces a 15-
600 kilodalton protein exhibiting marked homology to ubiquitin. *The Journal*
601 *of biological chemistry* 262:11315-11323.
602 Hansen, T.R., and J.K. Pru. 2014. ISGylation: a conserved pathway in mammalian
603 pregnancy. *Adv Exp Med Biol* 759:13-31.
604 Henkes, L.E., J.K. Pru, R.L. Ashley, R.V. Anthony, D.N. Veeramachaneni, K.C. Gates,
605 and T.R. Hansen. 2015. Embryo mortality in Isg15-/- mice is exacerbated
606 by environmental stress. *Biol Reprod* 92:36.
607 Hermann, M., and D. Bogunovic. 2017. ISG15: In Sickness and in Health. *Trends*
608 *Immunol* 38:79-93.
609 Knight, E., Jr., D. Fahey, B. Cordova, M. Hillman, R. Kutny, N. Reich, and D.
610 Blomstrom. 1988. A 15-kDa interferon-induced protein is derived by
611 COOH-terminal processing of a 17-kDa precursor. *The Journal of biological*
612 *chemistry* 263:4520-4522.
613 Loeb, K.R., and A.L. Haas. 1992. The interferon-inducible 15-kDa ubiquitin
614 homolog conjugates to intracellular proteins. *The Journal of biological*
615 *chemistry* 267:7806-7813.

616 Ma, W., W. Lim, K. Gee, S. Aucoin, D. Nandan, M. Kozlowski, F. Diaz-Mitoma, and A.
617 Kumar. 2001. The p38 mitogen-activated kinase pathway regulates the
618 human interleukin-10 promoter via the activation of Sp1 transcription
619 factor in lipopolysaccharide-stimulated human macrophages. *The Journal*
620 *of biological chemistry* 276:13664-13674.
621 McNab, F., K. Mayer-Barber, A. Sher, A. Wack, and A. O'Garra. 2015. Type I
622 interferons in infectious disease. *Nature reviews. Immunology* 15:87-103.
623 Morales, D.J., and D.J. Lenschow. 2013. The antiviral activities of ISG15. *Journal of*
624 *molecular biology* 425:4995-5008.
625 Nair, S., P.A. Ramaswamy, S. Ghosh, D.C. Joshi, N. Pathak, I. Siddiqui, P. Sharma,
626 S.E. Hasnain, S.C. Mande, and S. Mukhopadhyay. 2009. The PPE18 of
627 Mycobacterium tuberculosis interacts with TLR2 and activates IL-10
628 induction in macrophage. *Journal of immunology* 183:6269-6281.
629 Narasimhan, J., J.L. Potter, and A.L. Haas. 1996. Conjugation of the 15-kDa
630 interferon-induced ubiquitin homolog is distinct from that of ubiquitin.
631 *The Journal of biological chemistry* 271:324-330.
632 Novais, F.O., L.P. Carvalho, S. Passos, D.S. Roos, E.M. Carvalho, P. Scott, and D.P.
633 Beiting. 2015. Genomic profiling of human Leishmania braziliensis lesions
634 identifies transcriptional modules associated with cutaneous
635 immunopathology. *The Journal of investigative dermatology* 135:94-101.
636 Owhashi, M., Y. Taoka, K. Ishii, S. Nakazawa, H. Uemura, and H. Kambara. 2003.
637 Identification of a ubiquitin family protein as a novel neutrophil
638 chemotactic factor. *Biochemical and biophysical research communications*
639 309:533-539.
640 Potter, J.L., J. Narasimhan, L. Mende-Mueller, and A.L. Haas. 1999. Precursor
641 processing of pro-ISG15/UCRP, an interferon-beta-induced ubiquitin-like
642 protein. *The Journal of biological chemistry* 274:25061-25068.
643 Recht, M., E.C. Borden, and E. Knight, Jr. 1991. A human 15-kDa IFN-induced
644 protein induces the secretion of IFN-gamma. *Journal of immunology*
645 147:2617-2623.
646 Rider, P., E. Voronov, C.A. Dinarello, R.N. Apte, and I. Cohen. 2017. Alarmins: Feel
647 the Stress. *Journal of immunology* 198:1395-1402.
648 Schoggins, J.W., and C.M. Rice. 2011. Interferon-stimulated genes and their
649 antiviral effector functions. *Current opinion in virology* 1:519-525.
650 Skaug, B., and Z.J. Chen. 2010. Emerging role of ISG15 in antiviral immunity. *Cell*
651 143:187-190.
652 Skrzeczynska-Moncznik, J., M. Bzowska, S. Loseke, E. Grage-Griebenow, M.
653 Zembala, and J. Pryjma. 2008. Peripheral blood CD14high CD16+
654 monocytes are main producers of IL-10. *Scandinavian journal of*
655 *immunology* 67:152-159.
656 Speake, C., S. Presnell, K. Domico, B. Zeitner, A. Bjork, D. Anderson, M.J. Mason, E.
657 Whalen, O. Vargas, D. Popov, D. Rinchai, N. Jourde-Chiche, L. Chiche, C.
658 Quinn, and D. Chaussabel. 2015. An interactive web application for the
659 dissemination of human systems immunology data. *Journal of*
660 *translational medicine* 13:196.
661 Tamassia, N., M. Zimmermann, M. Castellucci, R. Ostuni, K. Bruderek, B. Schilling,
662 S. Brandau, F. Bazzoni, G. Natoli, and M.A. Cassatella. 2013. Cutting edge:
663 An inactive chromatin configuration at the IL-10 locus in human
664 neutrophils. *Journal of immunology* 190:1921-1925.

665 Tecalco Cruz, A.C., and K. Mejia-Barreto. 2017. Cell type-dependent regulation of
666 free ISG15 levels and ISGylation. *J Cell Commun Signal*
667 Teles, R.M., T.G. Graeber, S.R. Krutzik, D. Montoya, M. Schenk, D.J. Lee, E.
668 Komisopoulou, K. Kelly-Scumpia, R. Chun, S.S. Iyer, E.N. Sarno, T.H. Rea, M.
669 Hewison, J.S. Adams, S.J. Popper, D.A. Relman, S. Stenger, B.R. Bloom, G.
670 Cheng, and R.L. Modlin. 2013. Type I interferon suppresses type II
671 interferon-triggered human anti-mycobacterial responses. *Science*
672 339:1448-1453.
673 Wang, B.X., S.A. Grover, P. Kannu, G. Yoon, R.M. Laxer, E.A. Yeh, and E.N. Fish.
674 2017a. Interferon-Stimulated Gene Expression as a Preferred Biomarker
675 for Disease Activity in Aicardi-Goutieres Syndrome. *Journal of interferon &*
676 *cytokine research : the official journal of the International Society for*
677 *Interferon and Cytokine Research* 37:147-152.
678 Wang, P., H. Qi, S. Song, S. Li, N. Huang, W. Han, and D. Ma. 2015a. ImmuCo: a
679 database of gene co-expression in immune cells. *Nucleic acids research*
680 43:D1133-1139.
681 Wang, P., Y. Yang, W. Han, and D. Ma. 2015b. ImmuSort, a database on gene
682 plasticity and electronic sorting for immune cells. *Scientific reports*
683 5:10370.
684 Wang, W., Y. Yin, L. Xu, J. Su, F. Huang, Y. Wang, P.P.C. Boor, K. Chen, W. Wang, W.
685 Cao, X. Zhou, P. Liu, L.J.W. van der Laan, J. Kwekkeboom, M.P.
686 Peppelenbosch, and Q. Pan. 2017b. Unphosphorylated ISGF3 drives
687 constitutive expression of interferon-stimulated genes to protect against
688 viral infections. *Science signaling* 10:
689 Zhang, X., D. Bogunovic, B. Payelle-Brogard, V. Francois-Newton, S.D. Speer, C.
690 Yuan, S. Volpi, Z. Li, O. Sanal, D. Mansouri, I. Tezcan, G.I. Rice, C. Chen, N.
691 Mansouri, S.A. Mahdaviani, Y. Itan, B. Boisson, S. Okada, L. Zeng, X. Wang,
692 H. Jiang, W. Liu, T. Han, D. Liu, T. Ma, B. Wang, M. Liu, J.Y. Liu, Q.K. Wang, D.
693 Yalnizoglu, L. Radoshevich, G. Uze, P. Gros, F. Rozenberg, S.Y. Zhang, E.
694 Jouanguy, J. Bustamante, A. Garcia-Sastre, L. Abel, P. Lebon, L.D.
695 Notarangelo, Y.J. Crow, S. Boisson-Dupuis, J.L. Casanova, and S. Pellegrini.
696 2015. Human intracellular ISG15 prevents interferon-alpha/beta over-
697 amplification and auto-inflammation. *Nature* 517:89-93.
698

699

700

Figure 1

Dos Santos *et. al* 2017

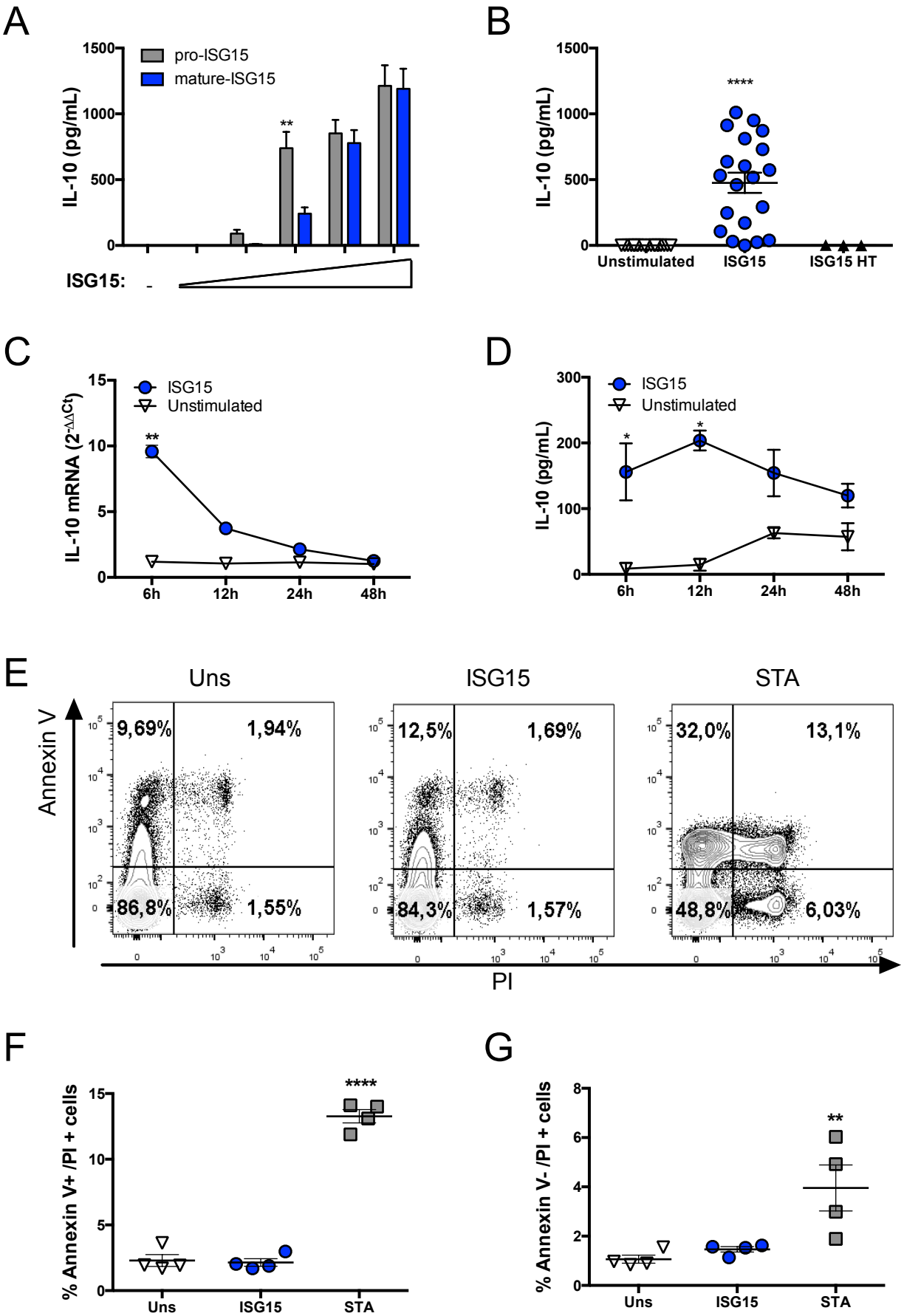

Figure 2

Dos Santos *et. al* 2017

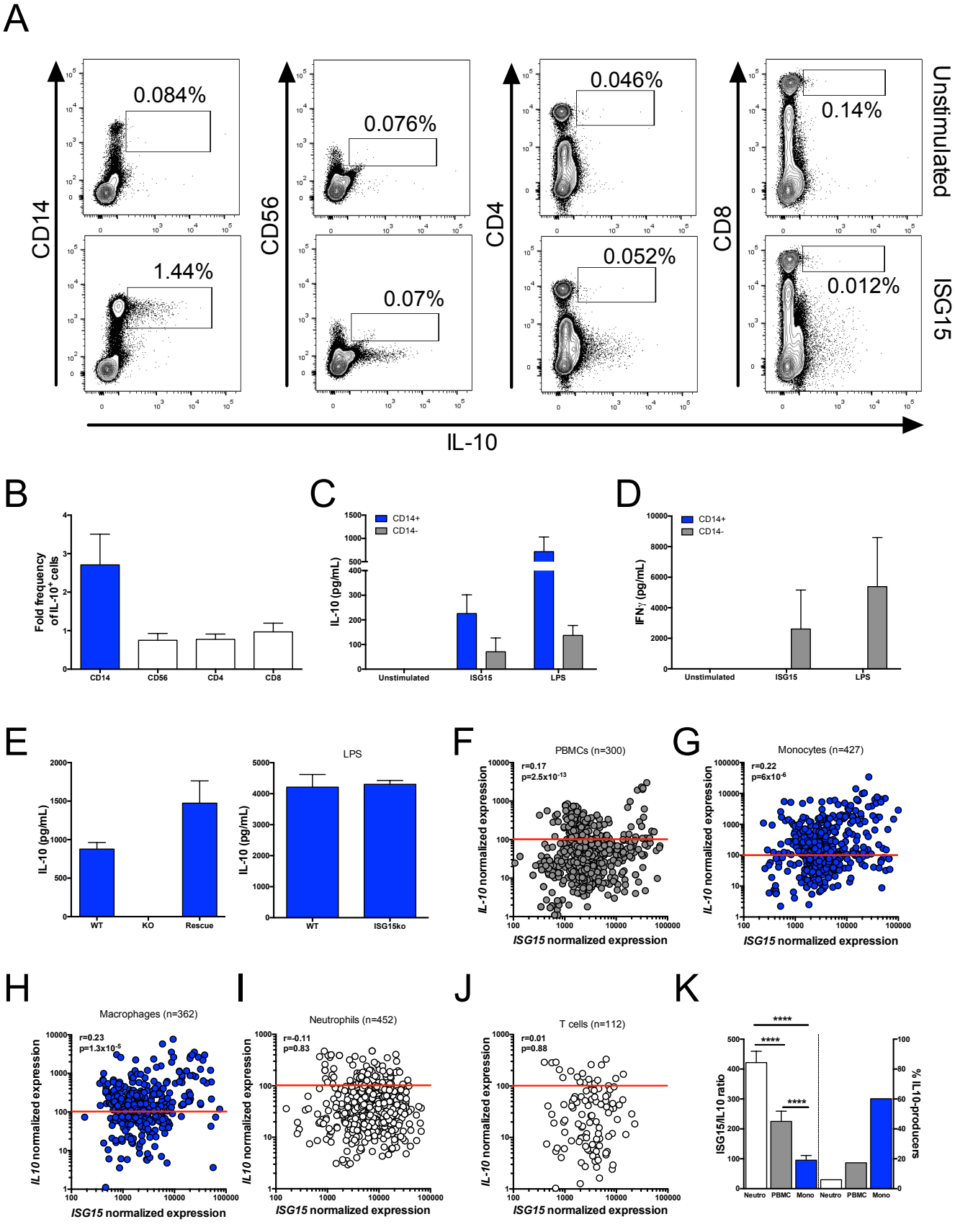

Figure 3

Dos Santos *et. al* 2017

A

Gene symbol	p value	logFC LAT	logFC ACT	p value
ISG15	0.0142	-1.00	1.99	7x10-6
IL10	0.0040	-0.62	0.34	0.0324
IFNG	0.0931	0.45	-0.52	0.0556
CD14	0.0857	-0.23	0.81	1x10-5
CD4	0.0012	-0.57	0.06	0.7990
CD8A	0.0004	0.86	-1.32	0.0008
NCAM1	0.0370	1.18	-0.47	0.0382
MAPK1	0.1480	0.25	0.37	0.0029
MAPK14	0.0019	0.86	1.02	0.0004
MAPK3	0.0001	-0.52	0.72	0.0002
PIK3CA	0.0228	-4.45	3.79	0.0872
STAT1	0.2800	-0.19	1.41	6x10-9
STAT2	0.0940	-0.27	1.07	3x10-8
STAT3	0.0025	-0.35	0.60	0.0001
STAT4	0.5900	0.06	-0.64	0.0003

B

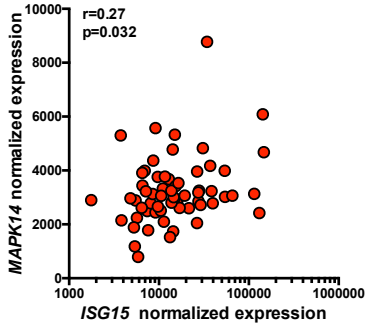

C

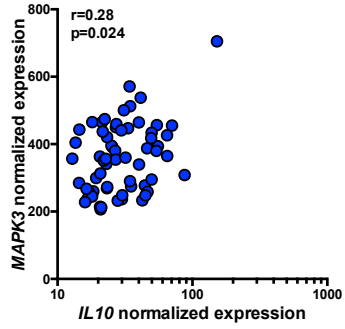

D

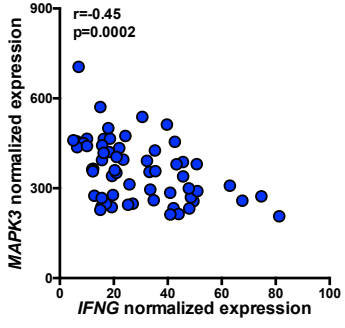

E

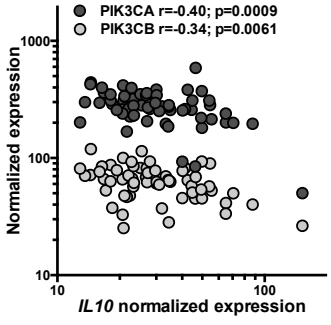

F

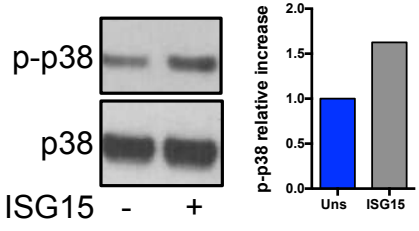

G

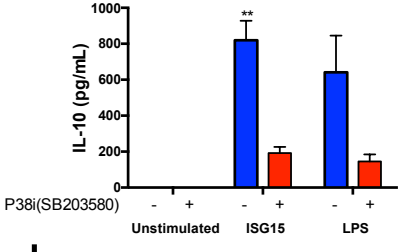

H

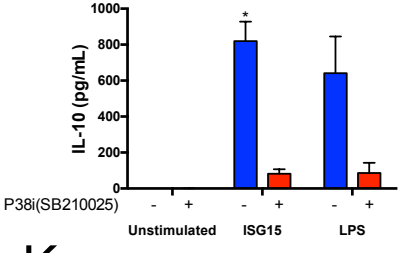

I

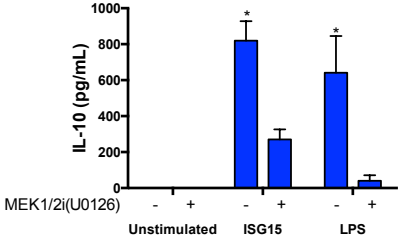

J

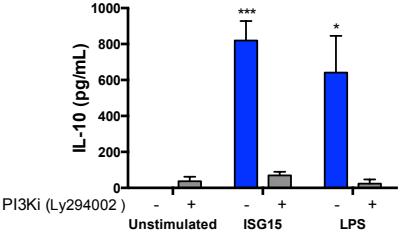

K

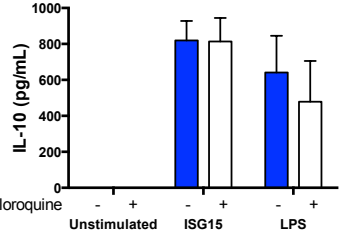

Figure 4
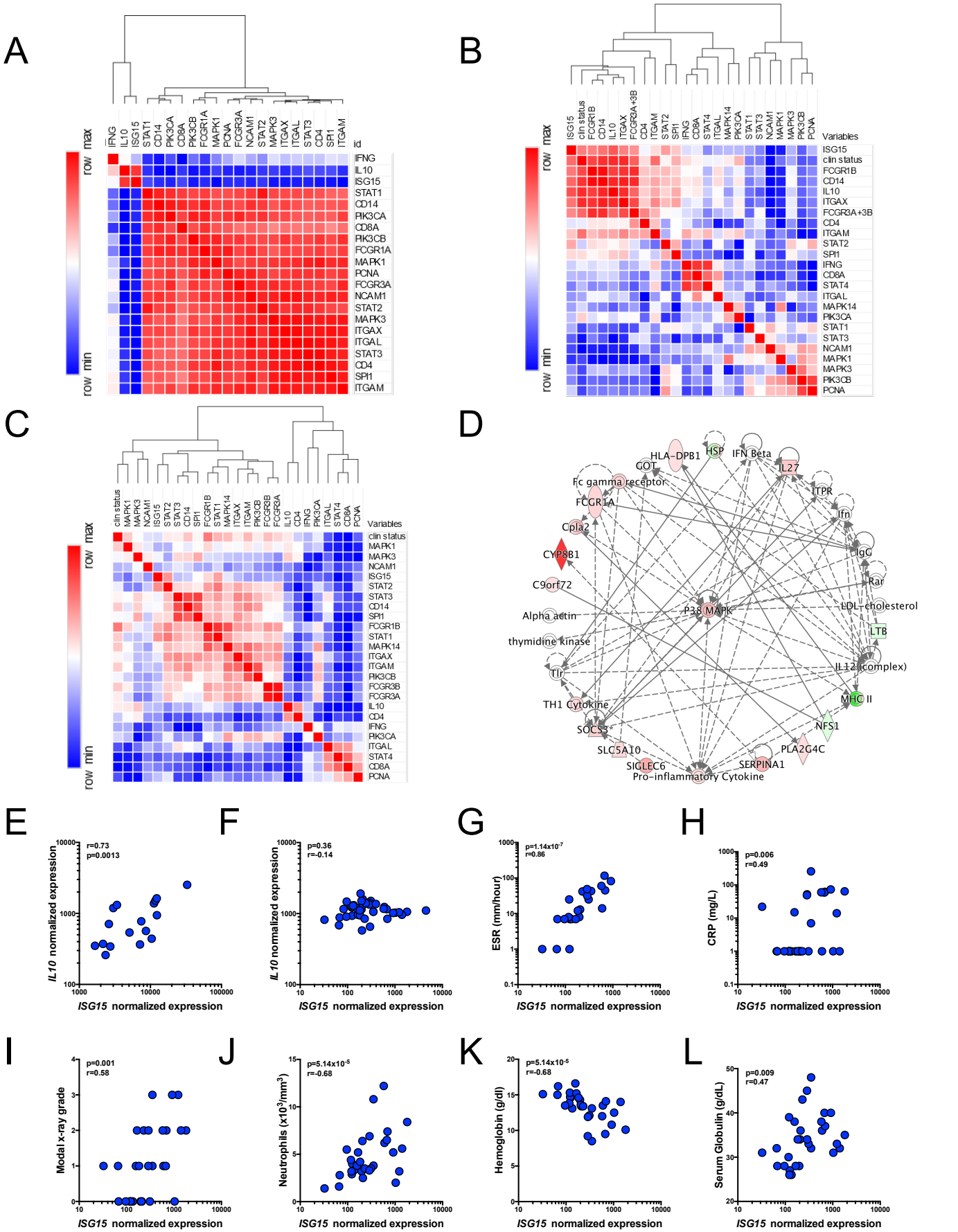
Dos Santos *et. al* 2017